Oxygen Bubble Templated Anodic Deposition of Porous PbO_2

Nicola Comisso, Sandro Cattarin, Paolo Guerriero, Luca Mattarozzi, Marco Musiani*, Enrico Verlato
IENI CNR, Corso Stati Uniti 4, 35127 Padova, Italy

Abstract

The oxygen bubble templated deposition of porous PbO_2 was realized by anodizing Pb(II) solutions (in nitrate-acetate, sulfamate or methanesulfonate media) at large current density. This process is the anodic analogue of the more common hydrogen bubble templated electrodeposition of porous metals. The porous PbO_2 layers consisted of a mixture of α- and β-phases, in contrast to compact layers deposited at low current density (pure α-PbO_2). The void volume fraction of porous PbO_2 was estimated.

Keywords: oxygen evolution, porosity, electrodeposition, methanesulfonic acid

* Corresponding Author. E-mail: m.musiani@ieni.cnr.it

Introduction

The hydrogen bubble templated electrodeposition of porous metals and alloys has been extensively investigated, in recent years [1]. In this process, an electrolysis performed at high current density causes simultaneous metal ions reduction and hydrogen evolution, leading to the formation onto the cathode of highly porous metal films, normally consisting of nanocrystals. Some metals, like e.g. Sn [2], Ru [3] and Cu [4], have been converted to their oxides through annealing steps, maintaining their original bimodal porosity. In principle, metal oxide porous films might be produced directly at the anode, by oxidation of low-valence cations, under conditions of intense oxygen evolution. To the best of our knowledge, such a process, which would be the anodic analogue of hydrogen bubble template cathodic deposition of metals, has never been explored. Therefore, we undertook the investigation described below, aimed at realizing the oxygen bubble templated anodic deposition of porous PbO_2. Owing to possible uses of PbO_2 in energy storage and as inexpensive anode material, obtaining this oxide with a high surface roughness may be of practical interest [5, 6].

Experimental

Most PbO_2 layers were electrodeposited under galvanostatic control, in a 0.20 M $Pb(CH_3SO_3)_2$, 1.1 M CH_3SO_3H electrolyte, onto Ni face-down RDEs (0.317 cm^{-2}, 900 min^{-1}) using a single-compartment cell, with a Pb sheet counterelectrode, at 25°C. PbO_2 layers used for the measurement of their thickness (by SEM) and in XRD experiments, were deposited onto vertical Ni sheet electrodes (1 cm^2). Ahead of applying the large j_D expected to cause the growth of porous oxide, a thin PbO_2 film (deposition charge Q_D = 1 C cm^{-2}) was deposited onto Ni electrodes, polished with abrasive paper, at low current density (j_D = 0.02 A cm^{-2}), to improve the adhesion. Two other electrolytes were also tested: (i) 0.45 M $PbNO_3$, 0.065 M $Pb(CH_3COO)_2$, (ii) 0.50 M $Pb(NH_2SO_3)_2$, 0.20 M NH_2SO_3H.

Electrochemical tests were performed with an Autolab PGSTAT 302N. Morphologies of the PbO_2 films were determined with a FEG-ESEM FEI Quanta 200 F instrument, equipped with a field emission gun, operating in high vacuum conditions. X-Ray

diffractograms were obtained with a Philips X-PERT PW3710 diffractometer, employing a CuKα source (40 kV, 30 mA).

Results and discussion

Figures 1a-b show that porous PbO_2 layers were obtained in CH_3SO_3H medium, at large current density. They adhered well to Ni and, besides pores with a mouth diameter of a few micrometres, exhibited some cracks. Comparable layers were deposited from nitrate-acetate or sulfamate baths, but using these media some detachment was observed. Formation of powders was negligible in all media. Figure 1c, obtained with a larger magnification, reveals a microcrystalline, rather compact structure of PbO_2, and no a nano-scale porosity comparable to that of metal deposits. This result is ascribed to different electrocrystallization kinetics of PbO_2, as compared to metals, and to its lower tendency to undergo dendritic growth. The cross-sectional image in Figure 1d shows pores as deep as the layer thickness and somewhat branched. This SEM study suggested PbO_2 to have a lower void volume fraction and less strongly interconnected neighbouring pores than most porous metal layers described in the literature [1-4].

The void volume fraction, computed from the deposit mass (M) and volume (V) as:

$$f_V = 1 - \frac{M}{\rho V} = 1 - \frac{M}{\rho A d} \qquad (1)$$

where A is the electrode area, d the layer thickness and $\rho = 9.38$ g cm^{-3} the PbO_2 density, was found to be 0.56 and 0.52 at j_D = 1.0 and 3.0 A cm^{-2}, respectively. Typical values found for porous metals are 0.8 to 0.9.

To evaluate the current efficiency of the process, the PbO_2 layers were cathodically stripped in the CH_3SO_3H solution where they had been grown. Figure 2a shows the stripping voltammetries of layers deposited at j_D = 0.02, 0.50 and 3.0 A cm^{-2} and Q_D = 30 C cm^{-2}). The onset potential of the PbO_2 reduction was more positive when j_D was larger. At the end of the cathodic scan, a minor residual deposit was still detected on the Ni surface, in agreement with Li et al. [7]. The stripping charge was used to calculate the current efficiency of the deposition/stripping cycle, as a function of the deposition current density, shown in Figure 2b (full symbols). The empty symbols in the same figure, corresponding to efficiencies calculated from Q_D and M, show efficiencies

systematically higher by a few percent. The efficiency decline at larger j_D was obviously due to the stronger contribution of oxygen evolution. SEM images, see insets, showed that PbO_2 was compact when deposited at $j_D \leq 0.1$ A cm^{-2} (with efficiency $\geq 83\%$), and porous over the whole electrode surface at $j_D \geq 0.5$ A cm^{-2} (with efficiency $\leq 63\%$). For intermediate j_D values, a low density of pores, increasing from the centre to the edge of the electrode, was observed (images not shown).

Figure 3 compares the diffractograms obtained with PbO_2 layers deposited from a CH_3SO_3H solution at 0.20 (a) and 3.0 A cm^{-2} (b). The former closely corresponds to the diffractogram reported by Li et al. [7] for samples prepared at 25°C, and allows the identification of the product as α-PbO_2. The latter shows reflections typical of both α- and β-PbO_2, with the most intense one resulting from overlapping α–phase (130) and β-phase (211) lines. Diffractograms like that in figure 3b were obtained for all PbO_2 layers deposited at high current density (1.0 to 5.0 A cm^{-2}). PbO_2 phase changes as a function of experimental conditions were reported by other authors, e.g. [7,8]. Our results agree with the hypothesis that diffusion limited deposition of PbO_2 favours the β-phase [7].

With the aim of measuring the double layer capacity of PbO_2 layers, and hence their surface roughness factor, cyclic voltammograms were recorded in 0.1 M $NaNO_3$, in a 100 mV wide potential range centred at E = 1.05 V vs. Hg/Hg_2SO_4/0.5 M H_2SO_4 (corresponding to the open circuit potential), at different scan rates. Figure 4a shows four curves obtained with PbO_2 layers deposited at different j_D, with Q_D calculated to yield equal PbO_2 masses, on the basis of the efficiency-j_D dependence. The insets in Figure 4b show that the current, measured at E = 1.05 V, was proportional to scan rate, allowing the calculation of the capacity values plotted in Figure 4b, as a function of j_D. A major change in the capacity occurred around j_D = 0.2 A cm^{-2}, i.e. in the same j_D range where the deposits morphology changed from compact to porous, and their structure from α to α+β. At $j_D \geq 1.0$ A cm^{-2}, the capacity attained a quasi-constant value (0.19 F cm^{-2}) ca. 390 times higher than that measured for compact PbO_2 prepared with j_D = 0.02 A cm^{-2} (0.49 mF cm^{-2}). Figure 4c shows that, for samples prepared at j_D = 3 A cm^{-2}, the capacity increased linearly with Q_D.

The capacity measured with compact PbO_2 was much higher than double layer capacity values previously found for flat PbO_2/electrolyte interfaces ($\leq$ 0.06 mF cm^{-2}) [6]. This could suggest the contribution of a redox capacity, possibly associated with potential-

driven changes in the oxidation state of Pb in a non-stoichiometric lead oxide with O/Pb ratio < 2, although no redox peaks were visible in Figure 4a. Porosity could enhance the contribution of redox capacity, if species from the electrolyte were involved. A redox capacity could be suggested also by Figure 4c, although the linear capacity-thickness dependence was also compatible with a porosity essentially independent of the position along the PbO_2 layer thickness, causing a direct proportionality between thickness and surface area. Therefore, one cannot assume the capacity ratio 390 to be an accurate value of the surface roughness factor.

Figure 5a compares the voltammograms obtained by reducing compact and porous PbO_2 layers in H_2SO_4, to form $PbSO_4$ on their surface. Curves traced with the same colour denote layers with equal PbO_2 masses. Figure 5b shows that the reduction charge was independent of Q_D for the compact layers, and increased quasi-linearly with Q_D for the porous layers. For the thickest couple of layers in Figure 5a (12 mg cm^{-2}), the reduction charge was 11.6 times higher for porous than for compact PbO_2. In comparable experiments, Bartlett et al. [9] found a ratio ca. 7, for nanostructured macroporous vs. compact PbO_2. Considering that porous metal layers with nanostructured pore walls had surface roughness factors in the range 100-300, a value of 11.6 for PbO_2 seems compatible with the morphology shown by SEM.

Conclusions

The anodic electrodeposition of PbO_2 at large current densities, under conditions of vigorous oxygen evolution, yielded porous layers. Those deposited from methanesulfonate baths adhered well to Ni substrates. As compared to porous metal films produced with the hydrogen bubble templated electrodeposition method, PbO_2 films exhibited the micron-scale porosity induced by oxygen bubbles, but no nano-porosity. Their void volume fraction was higher than 0.5, but below the values typical of porous metals. Based on PbO_2 reduction charges for porous and compact layers surface roughness factor was estimate to be 11.5 to 16 (for 12 to 18 mg cm^{-2} deposits). Calculations based on capacity values yielded an unrealistically high surface roughness factor of 390. To the best of our knowledge, this paper is the first report on the anodic oxygen bubble templated deposition of a porous, electron-conducting oxide.

References

[1] B.J. Plowman, L.A. Jones, S.K. Bhargava, Chem. Comm. 51 (2015) 4331-4346.
[2] J.-H. Jeun, D.-H. Kim, S.-H. Hong, Sens. Actuators B 161 (2012) 784-790.
[3] M-G. Jeong, K. Zhuo, S. Cherevko, W.-J. Kim, C.-H. Chung, J. Power Sources 244 (2013) 806-811.
[4] S. Cherevko, C.-H. Chung, Talanta 80 (2010) 1371-1377.
[5] X Li, D. Pletcher, F.C. Walsh, Chem. Soc. Rev. 40 (2011) 3879-3894.
[6] U. Casellato, S. Cattarin, M. Musiani, Electrochim. Acta, 48 (2003) 3991-3998.
[7] X. Li, D. Pletcher, F.C. Walsh, Electrochim. Acta 54 (2009) 4688-4695.
[8] A.B. Velichenko, R. Amadelli, E.V. Gruzdeva, T.V. Luk'yanenko, F.I. Danilov, J. Power Sources 191 (2009) 103-110.
[9] P.N. Bartlett, T. Dunford, M.A. Ghanem, J. Mater. Chem. 12 (2002) 3130–3135.

Captions for Figures

Figure 1. SEM images of porous PbO_2 deposited in 0.20 M $Pb(CH_3SO_3)_2$, 1.1 M CH_3SO_3H electrolyte, at j_D = 3 A cm^{-2}.

Figure 2. (a) Stripping voltammograms of PbO_2 deposits in CH_3SO_3H medium. Scan rate 1 mV s^{-1}. (b) Dependence of the current efficiency of PbO_2 deposition on j_D, measured from stripping (full symbols) or gravimetric data (empty symbols). The insets show SEM images of layers deposited at j_D = 0.02 or 3.0 A cm^{-2}.

Figure 3. X-ray diffractograms of PbO_2 layers deposited from a methanesulfonate electrolyte at j_D = 0.02 A cm^{-2} (a) or at j_D = 3.0 A cm^{-2} (b).

Figure 4. Dependence of the capacity of PbO_2 layers on experimental variables. (a) effect of j_D on the cyclic voltammograms recorded in 0.1 M $NaNO_3$, scan rate 10 mV s^{-1}; (b) dependence of capacity on j_D, for a fixed PbO_2 deposit mass; (c) dependence of capacity on Q_D, for j_D = 3 A cm^{-2}. The insets in parts b and c show current-scan rate dependencies.

Figure 5. (a) Cyclic voltammograms recorded with compact (dashed lines) or porous (solid lines) PbO_2 layers in 1.0 M H_2SO_4, with a 10 mV s^{-1} scan rate; j_D and Q_D are reported on the figure. (b) Dependence of reduction charge on Q_D.

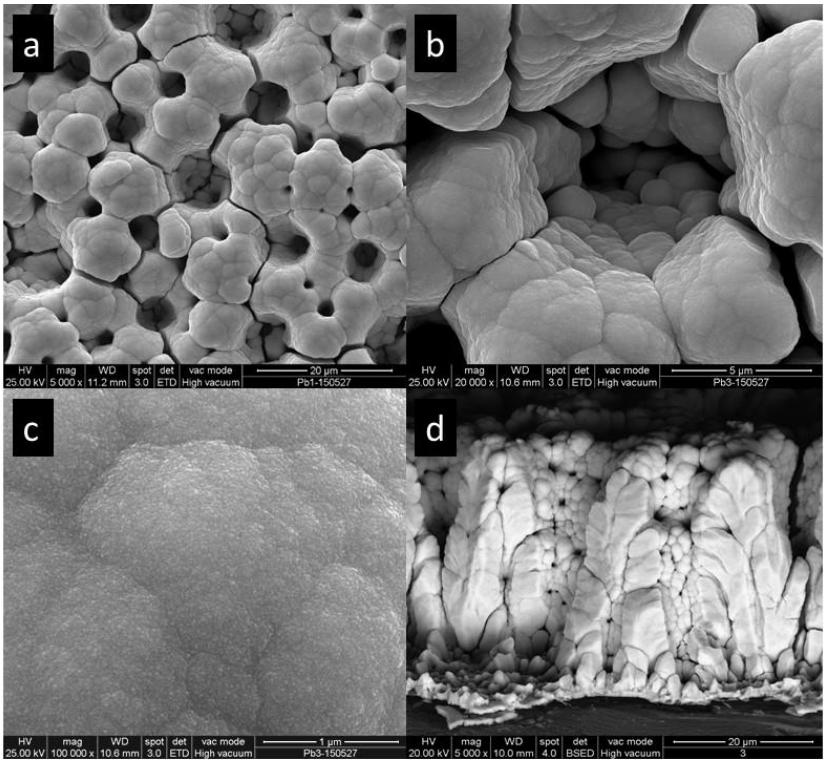
a
HV mag WD spot det vac mode
25.00 kV 5 000 x 11.2 mm 3.0 ETD High vacuum
20 µm
Pb1-150527
b
HV mag WD spot det vac mode
25.00 kV 20 000 x 10.6 mm 3.0 ETD High vacuum
5 µm
Pb3-150527
c
HV mag WD spot det vac mode
25.00 kV 100 000 x 10.6 mm 3.0 ETD High vacuum
1 µm
Pb3-150527
d
HV mag WD spot det vac mode
20.00 kV 5 000 x 10.0 mm 4.0 BSED High vacuum
20 µm
3

Figure 1.

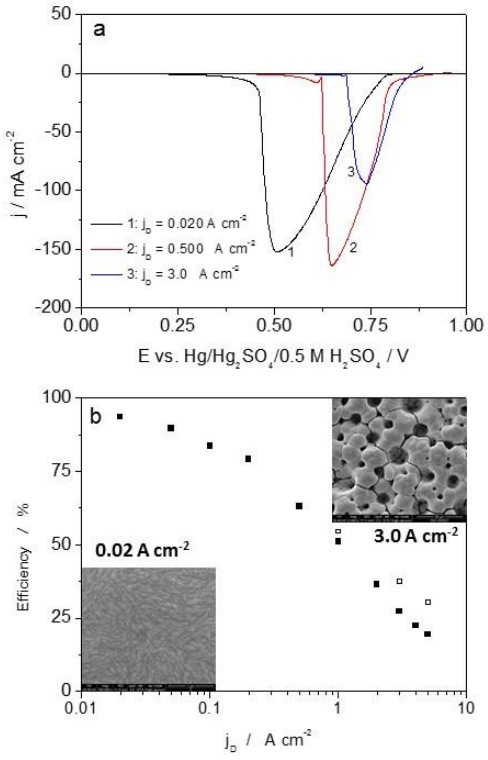
a
j / mA cm-2
E vs. Hg/Hg2SO4/0.5 M H2SO4 / V
1: jo = 0.020 A cm-2
2: jo = 0.500 A cm-2
3: jo = 3.0 A cm-2
b
Efficiency / %
jo / A cm-2
0.02 A cm-2
3.0 A cm-2

Figure 2

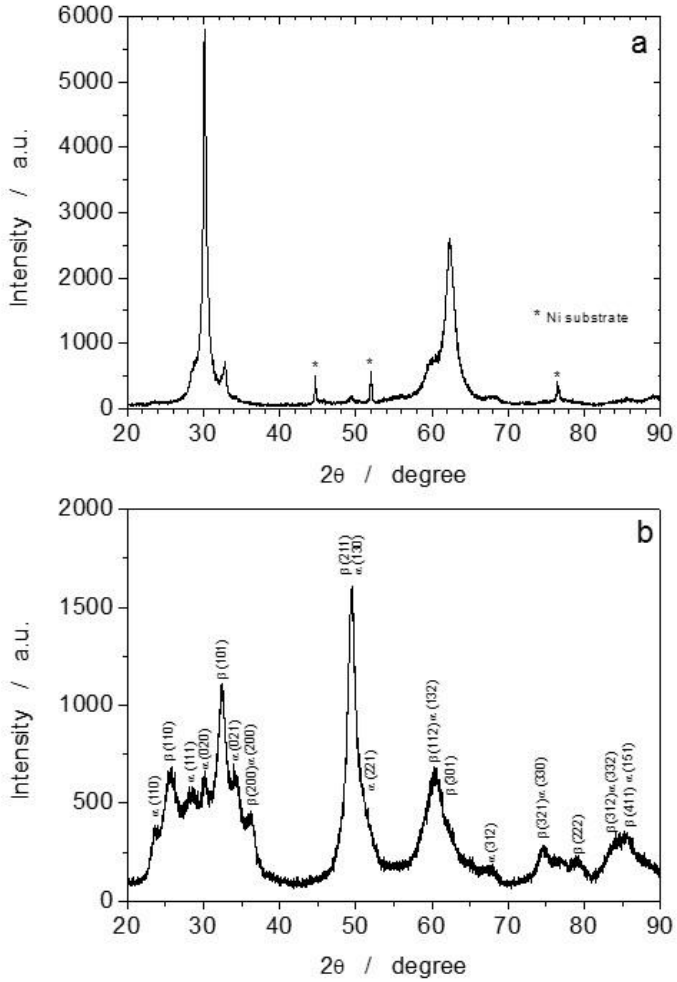
a
Intensity / a.u.
2θ / degree
* Ni substrate
b
Intensity / a.u.
2θ / degree
α (110)
β (110)
α (111)
α (020)
β (101)
α (021)
β(200)α (200)
β (211)
α (130)
α (221)
β(112)α (132)
β (301)
α (312)
β(321)α (330)
β (222)
β(312)α (332)
β (411) α (151)

Figure 3

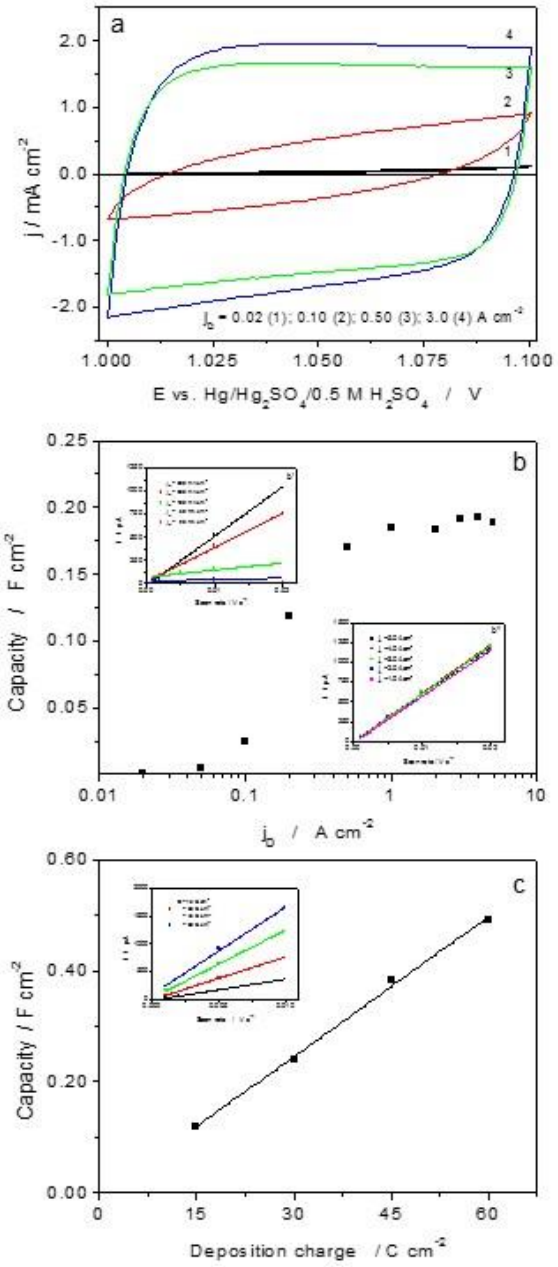
a
2.0
1.0
0.0
-1.0
-2.0
j / mA cm-2
4
3
2
1
jb = 0.02 (1); 0.10 (2); 0.50 (3); 3.0 (4) A cm-2
1.000
1.025
1.050
1.075
1.100
E vs. Hg/Hg2SO4/0.5 M H2SO4 / V
b
0.25
0.20
0.15
0.10
0.05
Capacity / F cm-2
0.01
0.1
1
10
jb / A cm-2
c
0.60
0.40
0.20
0.00
Capacity / F cm-2
0
15
30
45
60
Deposition charge / C cm-2

Figure 4

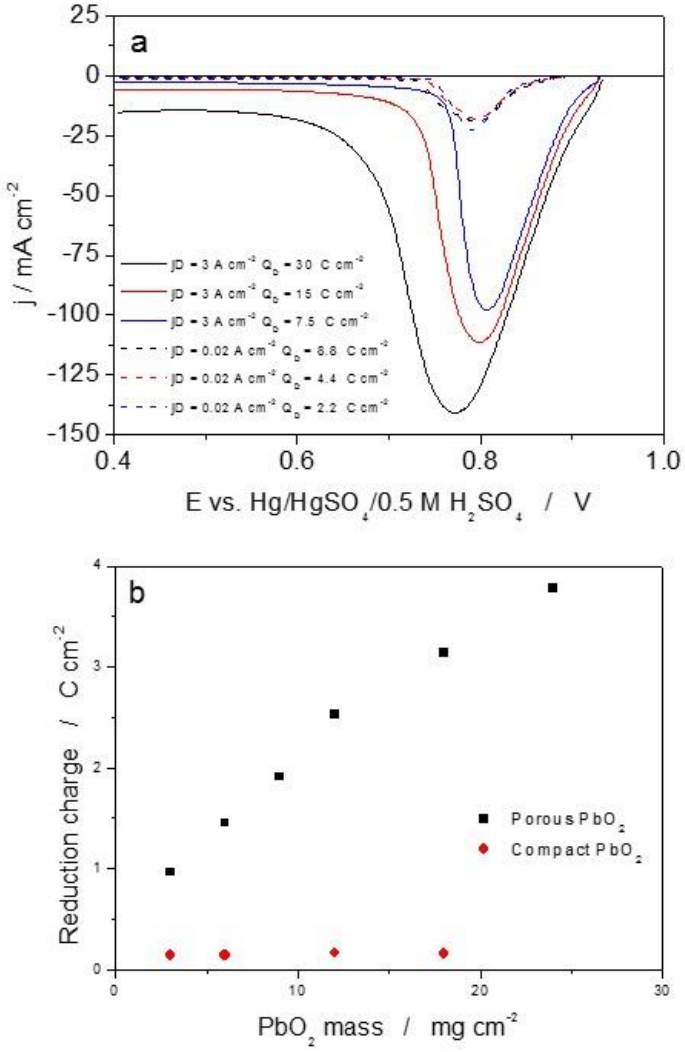
a
j / mA cm-2
E vs. Hg/HgSO4/0.5 M H2SO4 / V
jD = 3 A cm-2 QD = 30 C cm-2
jD = 3 A cm-2 QD = 15 C cm-2
jD = 3 A cm-2 QD = 7.5 C cm-2
jD = 0.02 A cm-2 QD = 8.8 C cm-2
jD = 0.02 A cm-2 QD = 4.4 C cm-2
jD = 0.02 A cm-2 QD = 2.2 C cm-2
b
Reduction charge / C cm-2
PbO2 mass / mg cm-2
Porous PbO2
Compact PbO2

Figure 5